Hindawi
Advances in Civil Engineering
Volume 2018, Article ID 8098242, 11 pages
https://doi.org/10.1155/2018/8098242

Research Article

Strengthening of Precast RC Frame to Mitigate Progressive Collapse by Externally Bonded CFRP Sheets Anchored with HFRP Anchors

Jianwu Pan, Xian Wang, and Fang Wu

Department of Civil Engineering, College of Aeronautics and Astronautics, Nanjing University of Aeronautics and Astronautics, Nanjing, Jiangsu 210016, China

Correspondence should be addressed to Xian Wang; 155931@qq.com

Received 8 September 2018; Revised 28 November 2018; Accepted 9 December 2018; Published 27 December 2018

Guest Editor: Li Chen

Currently, the robustness of precast reinforced concrete frames is attracting wide attention. However, avoiding "strong beams and weak columns" during strengthening against progressive collapse is a key problem. To discuss this problem, an experimental study on two 1/2-scale precast frame subassemblages under a pushdown loading regime was carried out in this paper. One specimen was strengthened with carbon fibre-reinforced polymer (CFRP) sheets on the beam sides. The middle parts of the CFRP sheets were anchored with hybrid fibre-reinforced polymer (HFRP) anchors. Another specimen was not strengthened. The failure mechanisms, failure modes, and strengthening effect are discussed. The strengthening effect is very obvious in the early catenary action stage. No shearing failure develops on HFRP anchors, which proves that the anchoring method is effective. Based on the experimental results, analytical models and preventive strengthening design and construction measures to mitigate progressive collapse of the precast RC frame are proposed.

1. Introduction

Although there is a very small probability of progressive collapse of structures [1], such collapse may cause serious consequences, such as the collapse of the Ronan Point Apartment in London in 1968 [2]. Recently, China has striven to develop precast buildings. Compared to the studies carried out on cast-in-place structures, limited studies have been carried out to research the behavior of precast concrete frames for prevention of progressive collapse. The studies on strengthening against progressive collapse are also necessary.

There are some studies on the progressive collapse resistance of precast concrete frame structures. Qian and Li [3] tested a series of three-dimensional precast structures with different connection types, including slab-beam connections and beam-column joints. In addition to the wet connections, Qian and Li [4] also tested precast concrete substructures with dry connections under a pushdown loading regime to investigate the effects of connection types on the behavior of precast concrete structures to mitigate progressive collapse. Kang and Tan et al. [5, 6] tested the precast frame subassemblages with a middle column removal and discussed the effects of engineered cementitious composites on progressive collapse resistance. Nimse et al. [7] studied the behavior of wet precast beam-column joints under progressive collapse scenario and concluded that all three precast joints were superior to the cast-in-place joint in terms of load capacity and ductility after strengthening the longitudinal rebar configuration. About the numerical simulation, Pan et al. [8] studied the behavior of beam-column joints and the progressive collapse performance of unbonded posttensioned precast concrete frame structures with finite element models which were established in OpenSEES, and Feng et al. [9] presented a numerical investigation of the progressive collapse behavior of the precast RC frame subassemblages. Some researchers have also conducted tests on strengthening against the progressive

collapse of structures [10–18]. Qian and Li [10, 11] tested a series of flat slab substructures to assess the effectiveness of proposed CFRP and GFRP strengthening schemes for improving the progressive collapse behavior. Kim et al. [12] tested ten RC beams to examine the effectiveness of the anchorage methods using CFRP anchors and/or U-wraps.

However, strengthening of precast RC structures against progressive collapse is a difficult problem, especially for structures that need to consider seismic performance simultaneously [19]. For structures with no problem of seismic performance but with insufficient progressive collapse resistance, the conventional strengthening methods for beams may cause "strong beams and weak columns" and weaken the seismic performance of structures. Then, columns have to be strengthened. Such a repeated process increases the cost significantly. To address this problem, in this study, we attempted to improve the traditional CFRP sheet strengthening method and tested the subassemblages of precast RC frames. Two assembled monolithic subassemblages of precast RC frames (scale = 1 : 2) were designed and constructed. One subassemblage was strengthened with CFRP sheets bonded on the beam sides, anchored with carbon fibre and steel fibre hybrid fibre-reinforced polymer (C/S HFRP) anchors, and compared with another unstrengthened specimen to discuss their progressive collapse resistance.

2. Experimental Content

2.1. Specimen Design. According to the local standard drawings of Shanghai (DBJT08-116-2013) [20], a four-floor concrete frame structure was designed. According to the requirements of the alternate load path method, a two-span subassemblage at the bottom floor was used as the research object. Two specimens were designed and constructed at a scale ratio of 1 : 2 (Figure 1). The specimens were made by the assembled monolithic method. The first concrete casting accomplished the precast part of beams, side columns, and seats, while the second concrete casting connected these members and filled concrete into beam-column joints and the upper parts of the beams. At the middle column joint, reinforcing bars of the beams were connected by full-grout sleeves. The reinforcing bars of beams used HRB400 with a diameter of 12 mm. The yield strength and ultimate strength of the reinforcing bars were 442 MPa and 617 MPa, respectively. The reinforcing bars of columns applied HRB400, which had a diameter of 14 mm. The stirrup was done using HPB300 with a diameter of 8 mm. The strength grade of the concrete was C40.

The stress mechanism of the beams throughout the collapse process can be divided into three action stages [1]: *flexural action (FA)*, *compressive arch action (CAA)*, and *catenary action (CA)*. The strengthened specimen had to make the CFRP sheets remain basically inactive in FA and CAA but work completely in CA. Hence, CFRP sheets with a single-layer width of 15 cm, a calculated thickness of 0.167 mm, and a tensile strength of 3243 MPa were bonded manually on the side surface of the beams continuously. At the two ends of side columns, steel plates and expansion bolts were used as anchors. Next, wedge blocks with a slope gradient of 0.1 were placed at 8 beam-column transitions by polymer concrete. HFRP anchors were applied along the CFRP sheets. Figure 2 shows the left half-span anchor arrangement. Each anchor (Figure 3) was formed by 12 bundles of carbon fibres (the length of the "root" part was 6 cm, and the diameter of the "umbrella" part was 6 cm). For each anchor, four pieces of 304 Cr–Ni stainless steel wires (diameter = 0.3 mm) were added.

2.2. Test Methods. To fully simulate the lateral tie force of columns during collapse and help the subassemblage enter the CA successfully, setting effective lateral constraints at the side columns of the two ends is extremely important. The triple lateral constraint shown in Figure 4 was adopted. Firstly, the base of the specimen was fixed on the test bench with channel steel members, steel plates, and screws; secondly, two channel steel members clamping side columns were installed; then, both ends of the channel steel members were fixed on the steel columns of the test bench; finally, two square steel tube members were supported on the channel steel members.

Displacement-controlled loading process was applied. When the actuator displacement was less than 40 mm, the loading process was applied at a very slow rate of 0.25 mm/min. When the displacement was between 40 mm and 104 mm, the loading process was carried out at a rate of 1.0 mm/min. When the displacement was greater than 104 mm, the loading process was implemented at a rate of 2 mm/min. Since the stroke of the actuator was 400 mm, unloading began at 400 mm. A 500 mm-high box iron impost was inserted between the actuator and middle column, and then, the reloading was carried out until the specimen finally collapsed. It should be noted that the short unload-reload curve is not plotted in Figure 6. The arrangement of the measuring points is shown in Figure 5. LC is the strain measuring point of concrete; LS is the strain measuring point of rebar; LM is the displacement measuring point; LP is the CFRP strain measuring point; LF is the force sensor; and LN is the measuring point in the channel steel members and square steel tube members in the lateral constraint.

3. Experimental Results

3.1. Load-Displacement Curves and Failure Process. The load-displacement curves at the middle column of the unstrengthened specimen and the strengthened specimen are shown in Figure 6. With increasing displacement, the subassemblage can be divided into three loading stages.

As shown in Figure 6, the OA segment on the curve is the FA stage. Microcracks with 0.01~0.05 mm width developed on the upper edges of the beams near the side columns and on the lower edges of the beams near the middle column.

The AB segment on the curve is the CAA stage. Cracks developed continuously and extended towards the middle span of the beams. Due to continuous cracking in the tensile regions, the neutral axis of the beams close to the side columns moved downward continuously, while the neutral

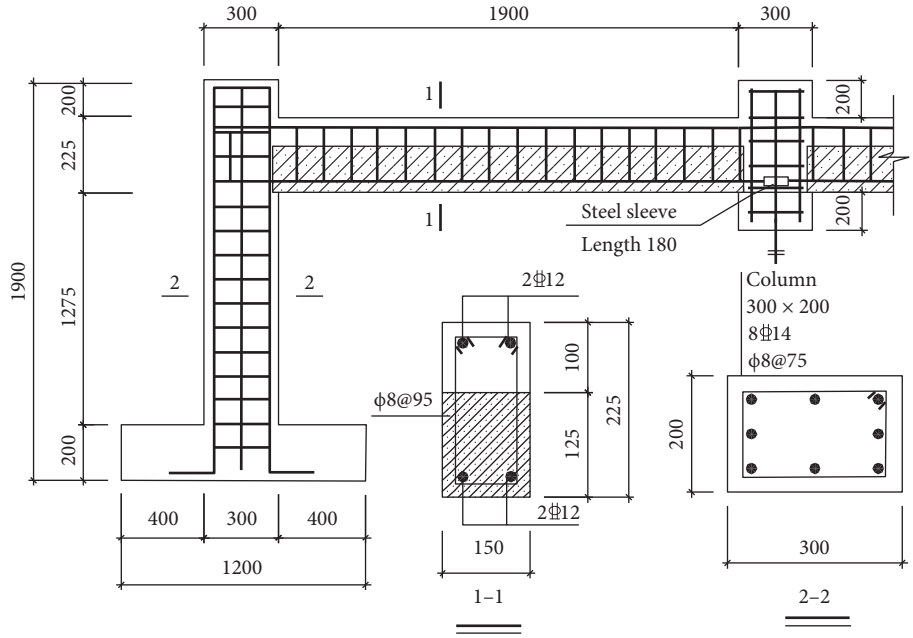

Figure 1: Details of the subassemblage.

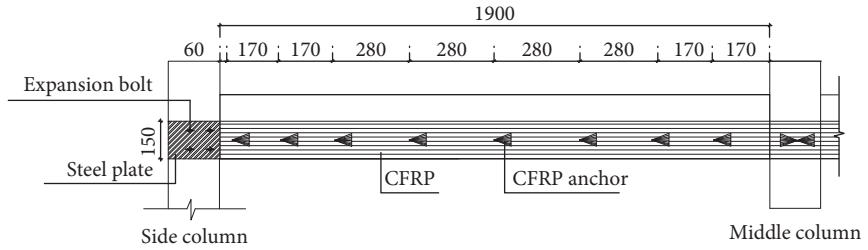

Figure 2: HFRP anchors arrangement.

(a) (b) (c) (d)

Figure 3: Details of the HFRP anchors. (a) Steel wires and carbon fibres, (b) HFRP anchors, (c) CFRP sheet and HFRP anchor, and (d) CFRP sheet anchored with HFRP anchors.

axis of the beams close to the middle column moved upward gradually, forming the compressive arch mechanism. The beams produced outward thrust, which made the side columns generate outward displacements. In the late CAA, tensile cracks extended continuously, and concrete in the compressive zone was crushed gradually, accompanied by the sound of concrete peeling off. The load capacity of the unstrengthened specimen decreased to 40 kN when the displacement of the middle column reached about 200 mm, and it was maintained between 40 kN and 50 kN. When the displacement exceeded 54.3 mm, the strengthened specimen developed the first CFRP local debonding. At this moment, the load was 61 kN. With constantly increasing displacement, the CFRP near the middle column produced the peeling sound continuously. The region with CFRP local debonding and local fracture expanded from the bottom

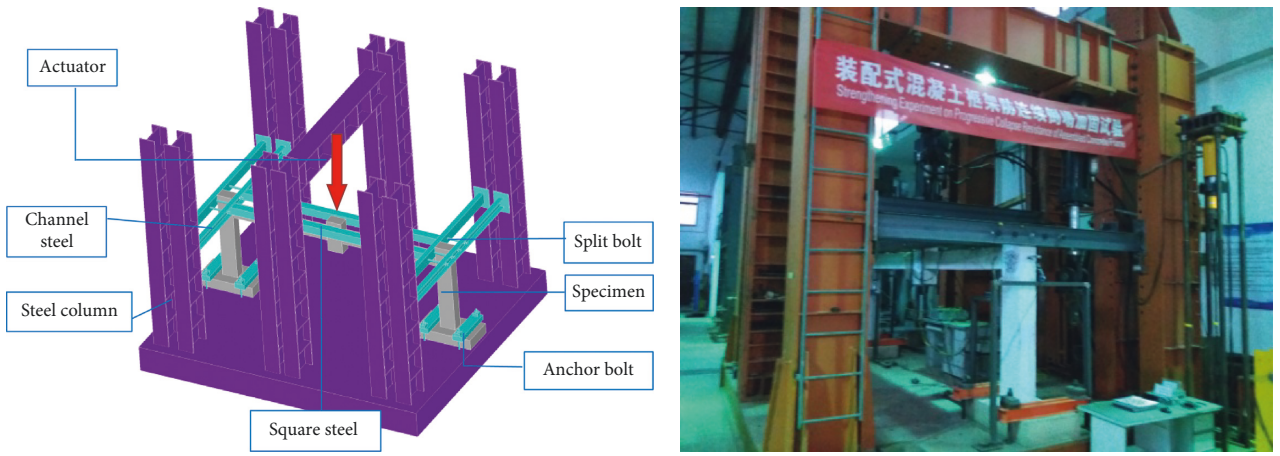

Figure 4: (a) Lateral constraint arrangement. (b) Side view of lateral constraint.

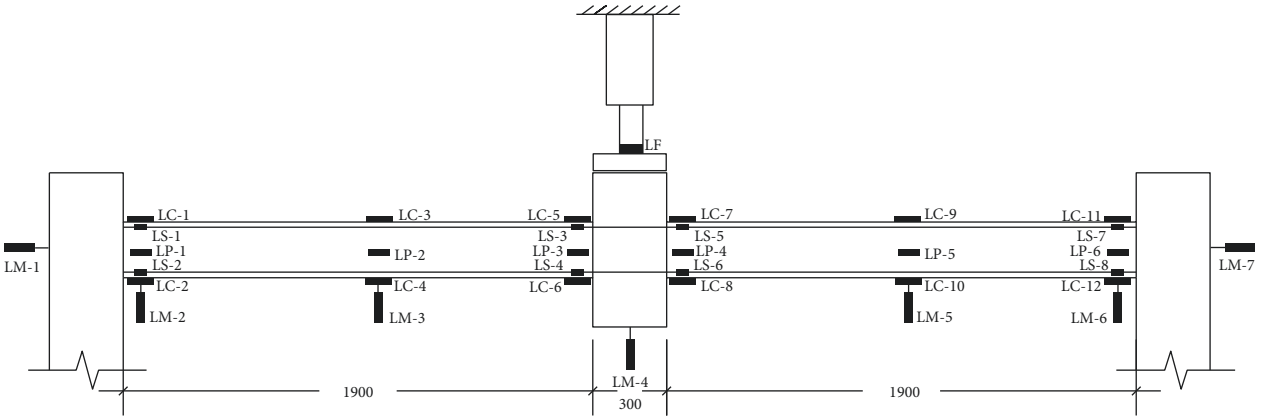

Figure 5: Measuring point arrangement.

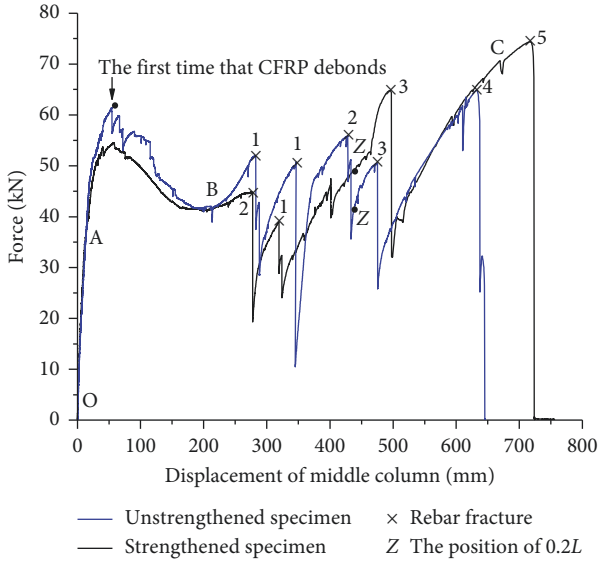

Figure 6: The load-displacement relation curves of the middle column. (1) Bottom rebar near the middle column. (2) Top rebar near the right column. (3) Top rebar near the left column. (4) Bottom rebar near the left column. (5) Top rebar near the middle column.

upward. When the displacement reached 70 mm and the load was 56.5 kN, the CFRP fracture region near the middle column exceeded to the HFRP anchor position. The displacement corresponding to the end point of CAA (point B) for the unstrengthened specimen and strengthened specimen was approximately 250 mm.

The BC segment on the curve is the CA stage. When the tensile crack extended through the whole concrete section, concrete in the compressive region was crushed completely. The load on the middle column was born entirely by the longitudinal reinforcement of the beams and the unbroken CFRP sheets. For the unstrengthened specimen, top bars of the right span were broken first when the displacement of the middle column reached 276 mm. The load capacity decreased sharply from 45 kN to 20 kN. Simultaneously, concrete in the compressive region of the beam produced abundant fragments. As displacement increased, the reinforcing bars of the beams fractured successively. Finally, with a loud sound, the specimen lost load capacity after all reinforcing bars of the beams fractured. At this moment, the displacement was 730 mm, and the load was 73 kN. For the CFRP strengthened specimen, some parts of CFRP sheets near the middle column were debonded and fractured when the subassemblage entered CAA (Figure 7(a)). CFRP debonding failure also occurred near the region of the umbrella part of the HFRP anchor close to the middle column (Figure 7(b)). When the displacement of the middle column reached 640 mm, the specimen finally collapsed. The ultimate collapse states of these two specimens are shown in Figures 8(a) and 8(b).

After failure of the subassemblages, the sleeves of reinforcing bars were removed and cut. No evident damage was observed in the sleeve section (Figure 9). Moreover, there was no evident damage on the cast-in-place and precast concrete interfaces. The progressive collapse failure process of the precast concrete subassemblage was the same as the progressive collapse failure process of the cast-in-place concrete subassemblage described in previous associated studies. This process was mainly divided into FA, CAA, and CA. No negative impacts were produced on the longitudinal rebar joint (grout sleeve) and the cast-in-place and precast concrete interfaces. In contrast, the sleeve arrangement in this test enhanced the anchor of the longitudinal rebar, which prevented anchor failure of the longitudinal rebar (pulling out of the longitudinal rebar) in experiments described in other studies. This result indicated that the subassemblage of the precast concrete frame was not inferior to the subassemblage of the cast-in-place concrete frame with the same reinforcement in terms of progressive collapse. However, reinforcement of precast concrete members is of the characteristic of "large rebar diameter and large rebar spacing." In other words, the number of reinforcing bars in the precast concrete member is lower than that in the cast-in-place concrete frame under the same reinforcement ratio. After CAA and CA, reinforcing bars in the structure developed tensile failure gradually. Hence, the number of reinforcing bars was negatively correlated with randomness of failure. This feature was one of the disadvantages of precast concrete structure.

Based on a comparison between the strengthened specimen and the unstrengthened specimen, the load capacities of the strengthened specimen in CAA and early CA were higher than those of the unstrengthened specimen. The first, second, and third rebar fracture points of the strengthened specimen appeared later than those of the unstrengthened specimen. The CFRP fractured completely when the middle column deformation reached 0.2 times the beam span (catenary ultimate deformation of structure regulated in DOD 2010 [21]). This result revealed that the strengthening scheme in this test achieved good effect. However, the result still had a certain mismatch with the expected effect (CFRP remained inactive or served slightly in FA and CAA but worked completely in CA). This situation was mainly caused by the downward bonding position of the CFRP sheets relative to the neutral axis of the beam and inadequate layers of the CFRP sheets. The ultimate deformation of the strengthened specimen was less than that of unstrengthened specimen, as shown in Figure 6. Because the fracture of reinforcing bars had some randomness, the ultimate deformation of specimens had some randomness, too.

The increase coefficient is defined as $\sum (\Delta P \cdot \Delta\delta)/\sum \Delta\delta$, where P and δ are the load and displacement of the middle column, respectively. The increase coefficient in different stages is shown in Figure 10. In FA, CFRP was almost inactive, and the increase coefficient was close to zero. The increase coefficients were 7.05% in CAA and 24.59% in CA, indicating that CFRP mainly played a role in CA. However, in this test, the CFRP sheets bore too much load in CAA and had to be improved in the further study.

3.2. Horizontal Displacements of Side Columns. In CAA, the side columns developed outward lateral displacements when the middle column moved downward. In CA, the side columns generated inward horizontal displacements. Therefore, changes in the axial force in the beam and conversion of the stress mechanism of the subassemblage could be deduced by observing the transformation between positive and negative horizontal displacements of the side columns. If the side column displacements were positive, columns moved outward. If the side column displacements were negative, columns moved inward. The side column displacements curves of the unstrengthened specimen and the strengthened specimen are shown in Figure 11.

In the whole loading process, the side column displacements of the unstrengthened specimen and the strengthened specimen ranged between 3 mm (outward) and −3 mm (inward). These results indicated that the lateral displacement constraint was very effective.

The strain curves of the square steel tube members in the lateral constraint are shown in Figure 12, which illustrates that the square steel tube members were pulled first and then compressed, and they accounted for approximately 10% of the displacement constraint. In the triple lateral constraints scheme (pulling-resistant ground anchors, antibending constraint of channel steel members,

(a) (b)

Figure 7: CFRP failure characteristics of the strengthened specimen near the middle column in CA. (a) CFRP debond and fracture. (b) CFRP debond.

(a) (b)

Figure 8: Collapse failure of the subassemblages. (a) CFRP strengthened specimen. (b) Unstrengthened specimen.

Figure 9: Sliced sleeve section.

and antistretching-compression constraint of square steel tube members), loads that were undertaken directly by the square steel tube members were relatively small and mainly played a role in enhancing the integrity and stability of constraints.

3.3. Strain of Rebar. Before the CA, the strain growth rates of reinforcing bars in the tensile region of beams were higher than those of reinforcing bars in the compression region. In the progressive collapse design, the deformation capacity of the beam end section can be increased by increasing the reinforcement ratio of the beam-column joint or adopting special structural measures. Since the CFRP shared some longitudinal rebar stress, the strain growth of the rebar in the strengthened specimen was lower than that in the unstrengthened specimen (Figure 13).

3.4. Strain of CFRP. In the collapse process, the principal cracks of the beam focused on the beam end near the beam-column joint, so the CFRP strain was also concentrated in these positions, showing a monotonic upward trend. The CFRP strain decreased near the middle of the beam span, and the strain in the middle beam span was compression first and then extension (Figure 14).

4. Analytical Models

4.1. Flexural Action Stage. In the FA stage, the analytical models for RC beams strengthened with CFRP sheets on the beam sides are relatively simple. Zhang et al. [22] proposed a practical design method. Chen et al. [23] also presented a practical calculation method. Chinese Strengthening Code [24] also gave the design method and construction suggestions for RC beams strengthened with CFRP sheets on the beam sides.

4.2. Compressive Arch Action Stage. The analytical models for the CAA stage are relatively complicated. Park and Gamble [25] proposed one of the most widely used CAA

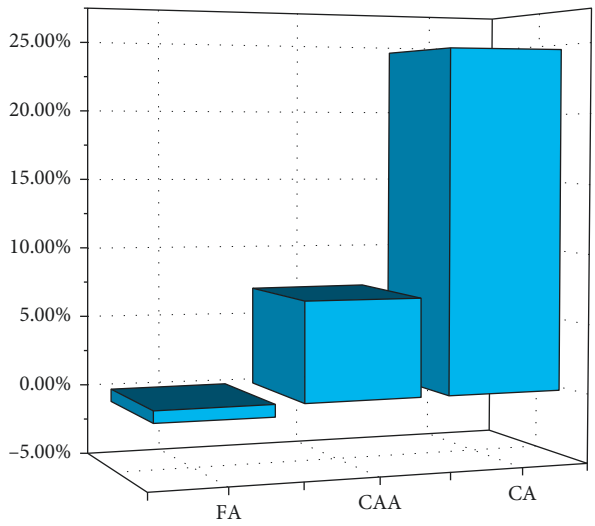

Figure 10: Increase coefficient of load capacity in different stages.

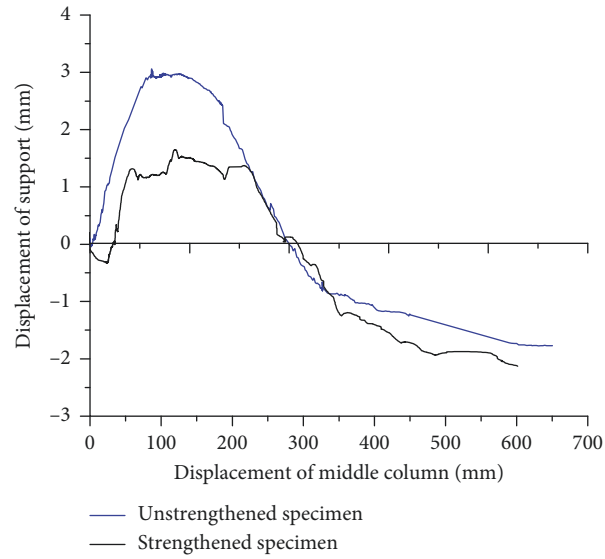

Figure 11: Relationship between lateral displacement of the side column and vertical displacement of the middle column.

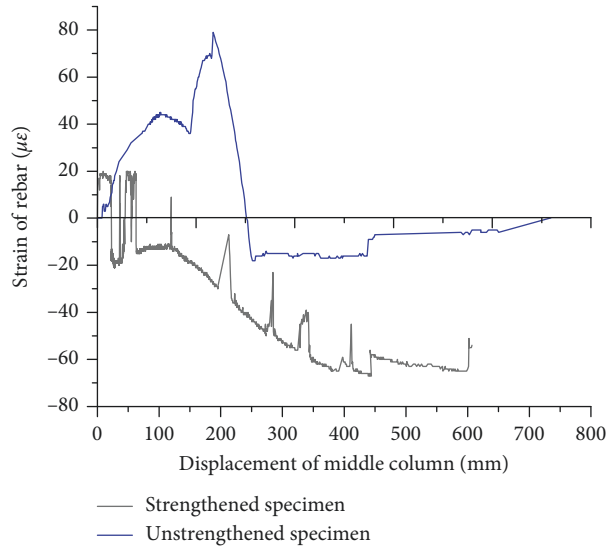

Figure 12: Strain on the square steel tube members.

analytical models. Park and Gamble's model was modified and validated by Su et al. [26] and Qian and Li [27]. Yu and Tan [28] and Kang and Tan [29] updated Park and Gamble's model by calculating iteratively the force-displacement relationship of RC beams at the CAA stage. Lu [30] also updated Park and Gamble's model for RC beams with and without slabs. Zeng [31] proposed a model to predict the CAA load capacity of FRP strengthened RC members. However, the CAA calculation model considering RC beams strengthened with CFRP sheets on the beam sides has not been reported in the relevant literature.

Park and Gamble's model is modified herein to be used for RC beams strengthened with CFRP sheets on the beam sides. It is assumed that (1) the compressive effect of the CFRP sheet is not considered and (2) the peak CAA displacements of the unstrengthened specimen and the strengthened specimen are the same. Then, based on Park and Gamble's model, when the width of the CFRP sheet is larger than $h-c$, the CAA load capacity of the strengthened specimen can be derived as follows:

$$\begin{aligned} P_{\mathrm{CAA}} = \frac{2}{\beta l}\Bigg\{ & 0.85 f_c' \beta_1 bh\left[\frac{h}{2}\left(1-\frac{\beta_1}{2}\right)+\frac{\delta}{4}(\beta_1-3)\right. \\ & +\frac{\delta^2}{8h}\left(2-\frac{\beta_1}{2}\right)+\frac{\beta l^2}{4\delta}(\beta_1-1)\varepsilon_t \\ & \left.+\frac{\beta l^2}{4h}\left(1-\frac{\beta_1}{2}\right)\varepsilon_t-\frac{\beta_1\beta^2 l^4}{16h\delta^2}\varepsilon_t^2\right] \\ & -\frac{\left(T'-T-C_s'+C_s-T_f\right)^2}{3.4 f_c' b}+\left(T'+T\right)\left(\frac{h}{2}-d'+\frac{\delta}{2}\right) \\ & +\left(C_s'+C_s\right)\left(\frac{h}{2}-d'-\frac{\delta}{2}\right)+T_f\left(\frac{h}{6}+\frac{c}{3}+\frac{\delta}{2}\right)\Bigg\}, \end{aligned} \tag{1}$$

where b and h are the width and height of the beam, respectively; f_c' is the concrete cylinder compressive strength; β_1 is the ratio of the depth of concrete equivalent stress block to the depth of the neutral axis; l is the total span; β is the ratio between the net span and the total span l; T, T_f, and T' are tensile resultant force of steel bars at the beam section near the middle column, tensile resultant force of CFRP sheets at the beam section near the middle column, and tensile resultant force of steel bars at the beam section near the side column, respectively; C_s and C_s' are compressive resultant forces of steel bars at the beam sections near the middle column and side column, respectively; d' is the thickness of the concrete cover; δ is the peak displacement corresponding to the peak load; c is the relative depth of the compression zone at the beam section near the middle

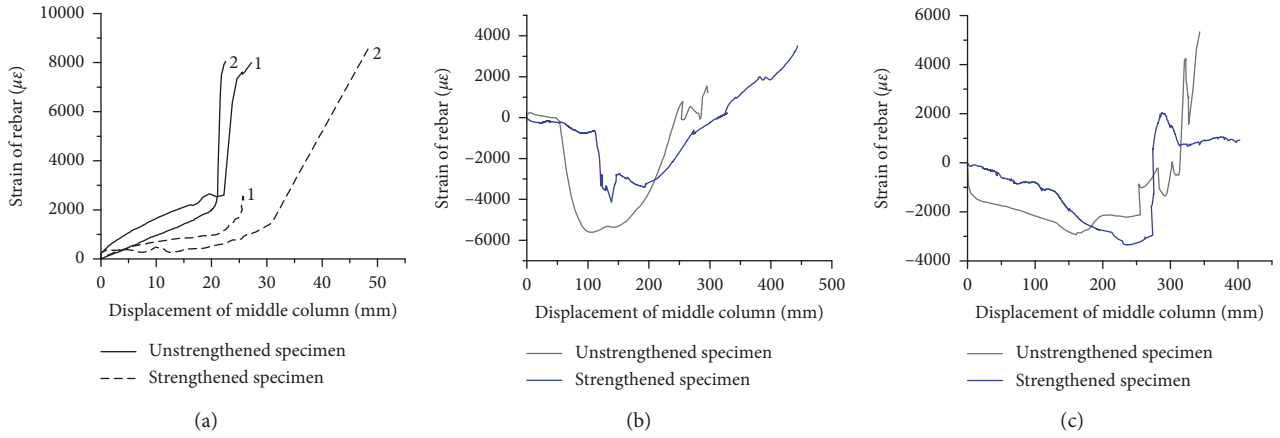

Figure 13: Strain of the longitudinal rebar on beam end sections of subassemblages. (a) Strain of (1) top rebar near side column and (2) bottom rebar near middle column. (b) Strain of bottom rebar near side column. (c) Strain of top rebar near middle column.

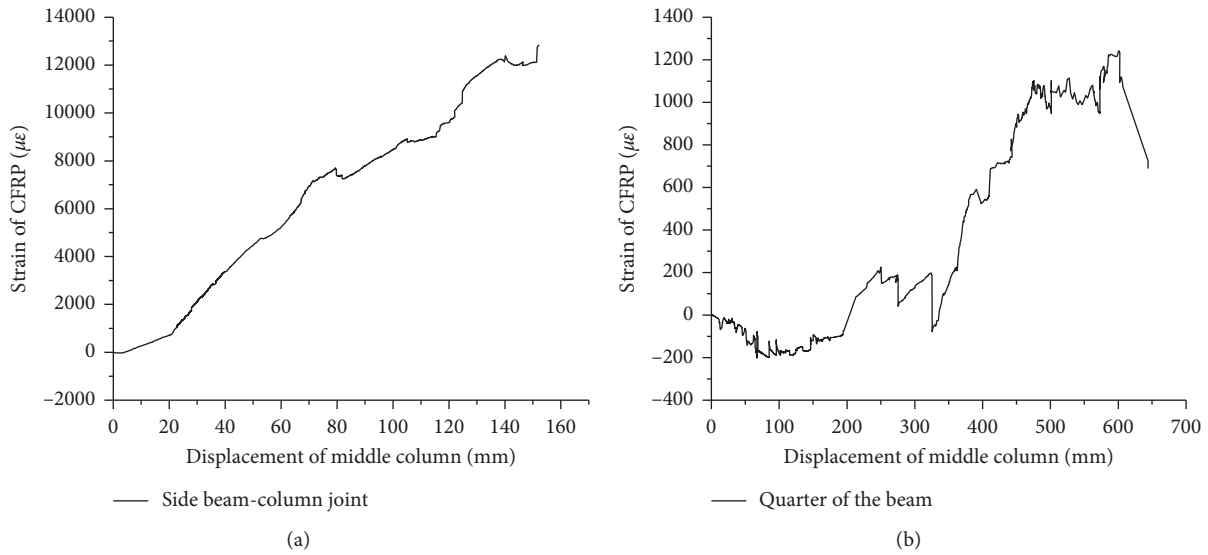

Figure 14: Strain of CFRP. (a) Strain of CFRP near the side column. (b) Strain of CFRP at 1/4 beam span.

column and is determined as shown in Equation (2); ε_t is the total axial strain due to beam axial deformation and support longitudinal displacement and is determined as shown in Equation (3):

$$c = \frac{h}{2} - \frac{\delta}{4} - \frac{\beta l^2}{4\delta}\varepsilon_t - \frac{T' - T - C_s' + C_s - T_f}{1.7 f_c' \beta_1 b}, \tag{2}$$

$$\varepsilon_t = \frac{\left(1/hE_c + (b/\beta l S)\right)\left[0.85 f_c' \beta_1 \left((h/2) - (\delta/4) - \left(T' - T - C_s' + C_s - T_f/1.7 f_c' \beta_1 b\right)\right) + \left(C_s - T - T_f/b\right)\right]}{1 + \left(0.85 f_c' \beta_1 \beta^3 l^2/\delta\right)\left((1/hE_c) + (b/\beta l S)\right)}, \tag{3}$$

where E_c is the concrete elastic modulus and S is the support rigidity in the horizontal direction.

Then, we can calculate the increment of load capacity with the following equation:

$$\Delta P_{\mathrm{CAA}} = P_{\mathrm{CAA}} - P_{\mathrm{CAA}}^{0}$$

$$= \frac{2}{\beta l}\left\{0.85 f_{\mathrm{c}}' \beta_1 bh\left[\frac{\beta l^2}{4\delta}(\beta_1 - 1)\left(\varepsilon_{\mathrm{t}} - \varepsilon_{\mathrm{t}}^{0}\right) + \frac{\beta l^2}{4h}\left(1 - \frac{\beta_1}{2}\right)\left(\varepsilon_{\mathrm{t}} - \varepsilon_{\mathrm{t}}^{0}\right) - \frac{\beta_1 \beta^2 l^4}{16h\delta^2}\left(\varepsilon_{\mathrm{t}}^{2} - \varepsilon_{\mathrm{t}}^{02}\right)\right]\right.$$

$$- \frac{\left(T' - T - C_{\mathrm{s}}' + C_{\mathrm{s}} - T_{\mathrm{f}}\right)^2 - \left(T' - T - C_{\mathrm{s}}' + C_{\mathrm{s}}\right)^2}{3.4 f_{\mathrm{c}}' b}$$

$$\left. + T_{\mathrm{f}}\left(\frac{h}{6} + \frac{c}{3} + \frac{\delta}{2}\right)\right\}, \quad (4)$$

where P_{CAA}^{0} and $\varepsilon_{\mathrm{t}}^{0}$ are the load capacity and the total axial strain due to beam axial deformation and support longitudinal displacement of the unstrengthened specimen, respectively.

For the experiment result of this paper, $\Delta P_{\mathrm{CAA}}^{\mathrm{exp}}$ is 7.29 kN, while $\Delta P_{\mathrm{CAA}}^{\mathrm{cal}}$ calculated with Equation (4) is 6.98 kN, and the relative error is −4%. The calculated value matches the test data very well. However, it should be noted that this result may be a coincidence, and more tests should be carried out to further prove the accuracy of Equation (4).

4.3. Catenary Action Stage. Yi and He [32] provided a simple analytical method to calculate the catenary action. Pham and Tan [33] also provided a simplified model of catenary action in reinforced concrete frames under axially restrained conditions. Alogla et al. [34] proposed an analytical model to predict the structural behavior of RC beams under column removal scenario considering the effect of bar fracture and the reduction in beam effective depth due to concrete crushing. However, the CA calculation model for RC beams strengthened with CFRP sheets on the beam sides has not been reported in literature.

In order to simplify the analysis, according to the catenary mechanism, we neglect the contribution of concrete to tension and only consider the tension of steel bars and FRP sheets, and we also assume that the anchorage of steel bars is in good condition and ignore the difference between precast concrete and cast-in-place concrete, so, when the catenary ultimate deformation occurs, the CA load capacity of the strengthened specimen is

$$P_{\mathrm{CA}} = P_{\mathrm{RC}} + P_{\mathrm{FRP}}, \quad (5)$$

where P_{RC} is the CA load capacity of the unstrengthened subassemblage [32] and P_{FRP} is the load capacity provided by the CFRP:

$$P_{\mathrm{RC}} = \frac{8\varphi\delta_m^3 E_t A_s}{L^3}, \quad (6)$$

where φ is the deformation adjustment coefficient of the rebar; δ_m is the catenary ultimate deformation, and its value is 0.2L according to existing codes (e.g., DOD 2010) [21]; E_{t} is Young's modulus of the beam; A_s is the longitudinal rebar sectional area, and L is the beam span:

$$P_{\mathrm{FRP}} = 2\gamma_s A_f f_{\mathrm{FRP}} \sin\theta, \quad (7)$$

where γ_s is the reduction coefficient of the load capacity. When $\delta_m \le 0.2\mathrm{L}$, $\gamma_s = 0.172$. In the experiment, we observed that CFRP developed local debonding and fracture in FA and CAA during actual loading, and the effective sectional area of the CFRP sheet decreased in CA. Therefore, the reduction coefficient of the load capacity of CFRP should be introduced. γ_s of the "designed CA" (between the beginning of CA and the time when the vertical displacement reached 0.2L) was calculated as 0.172 according to regression of test data. A_f is the sectional area of the CFRP sheet. f_{FRP} is the tensile strength of the CFRP sheet. $\sin\theta$ is the sine value of the beam end rotation when the vertical displacement of the middle column reached 0.2L, and its value is 0.196.

Therefore, the CA load capacity of the strengthened specimen can be determined from Equations (5)–(7):

$$P_{\mathrm{CA}} = 0.064\varphi E_t A_s + 0.392\gamma_s A_f f_{\mathrm{FRP}}. \quad (8)$$

It should be noted that the empirical coefficients of Equation (8) are only regressed from very limited test data, so more tests should be carried out to further improve the accuracy of Equation (8).

5. Construction Suggestions

For precast concrete beams, the anchorage of the longitudinal rebar can be enhanced by arranging sleeves reasonably, and attention should be paid to the treatment of the interface between cast-in-place and precast concrete.

(1) Bonding technology of CFRP sheets: CFRP sheets are suggested to bond to the beam side near the neutral axis of the beam. Slope processing should be applied at the beam-column transition. If the slope gradient is greater than 0.1, additional anchoring measures such as steel plate anchors should be employed. If the CFRP sheet is bonded on the lower or upper surface of the beam side, the corresponding verification should be implemented to avoid overall fracture of the CFRP sheet during FA or CAA. From the experimental results, the main stress areas of CFRP sheets are at both ends of the beams, so we can bond CFRP sheets and anchor HFRP anchors at both ends of the beams but not along the full span.

(2) Anchoring method of CFRP sheets: The goal of setting HFRP anchors is to avoid large-scale debonding failure of CFRP sheets in FA and CAA and successfully transit to CA. According to references [35, 36], the debonding load P_{FAN} of the CFRP sheet with HFRP anchors can be calculated as follows:

$$
\begin{aligned}
P_{\mathrm{FAN}} &= 0.427\beta_{\mathrm{p}}\beta_{\mathrm{L}}\sqrt{f_{\mathrm{c}}}b_{\mathrm{p}}l_{\mathrm{ae}},\\
l_{\mathrm{ae}} &= k_{\mathrm{am}}l_{\mathrm{e}},\\
L_{\mathrm{e}} &= \sqrt{\frac{E_{\mathrm{p}}t_{\mathrm{p}}}{\sqrt{f_{\mathrm{c}}}}},\\
\beta_{\mathrm{L}} &= \begin{cases} 1, & L_{\mathrm{f}} > L_{\mathrm{e}},\\ \sin\dfrac{\pi L_{\mathrm{f}}}{2L_{\mathrm{e}}}, & L_{\mathrm{f}} \le L_{\mathrm{e}}, \end{cases}\\
\beta_{\mathrm{p}} &= \sqrt{\frac{2-b_{\mathrm{p}}/b_{\mathrm{c}}}{1+b_{\mathrm{p}}/b_{\mathrm{c}}}},
\end{aligned}
\tag{9}
$$

where f_{c} is the concrete strength, b_{c} is the width of the concrete specimen, L_{f} is the bond length of CFRP, t_{p} is the calculated thickness of CFRP, b_{p} is the CFRP width, E_{p} is the elasticity modulus of CFRP, and k_{am} is the increase coefficient of the load capacity of the specimen. According to previous studies by our research team [37], k_{am} is suggested to be 1.6.

6. Conclusions

(1) The lateral constraint used in this paper is a triple constraint scheme, including the pulling-resistant ground anchors, antibending constraint of the channel steel members and antistretching-compression constraint of the square steel tube members. Test results prove that such lateral constraints are effective. The progressive collapse process of the assembled monolithic RC frame subassemblage is the same as that of the cast-in-place structure described in the previous literature and is also mainly divided into FA, CAA, and CA. The same phenomenon is observed in the strengthened subassemblage.

(2) No evident damage is observed at the longitudinal rebar connector (grout sleeve) and cast-in-place and precast concrete interfaces. Obviously, the assembled monolithic RC frame has no inherent disadvantage in progressive collapse resistance compared to the cast-in-place RC frame under the premise of equal reinforcement ratio and normal construction. However, the rebar of the precast concrete structure is of the characteristic of "large rebar diameter and large rebar spacing." In other words, the number of rebar in the precast concrete beam is lower than that in the cast-in-place concrete beam under the same reinforcement ratio. Rebar develop tensile failure gradually after CAA and CA. Therefore, the number of rebar is negatively correlated with the randomness of failure, which is one of the disadvantages of the precast RC frame.

(3) In this paper, a strengthened specimen with CFRP sheets bonded on the side surfaces of the beam is studied. The load capacity is not increased significantly in FA and CAA, which is advantageous for maintaining "strong columns and weak beams." The strengthening effect is very obvious in early CA. No shearing failure develops on HFRP anchors, which proves that the anchoring method is effective. Before the ultimate catenary deformation (0.2L) regulated by existing codes (e.g., DOD 2010), this strengthening scheme can meet engineering needs. However, when the deformation exceeds 0.2L, as the CFRP sheet fractures gradually, the CFRP sheets no longer work. Bonding CFRP sheets as close as possible to the neutral axis of the beam sides is suggested. Two-layer or more CFRP sheets or composite strengthening schemes, such as external bonding of CFRP sheets and near surface mounting (NSM) of CFRP rebar, should be used to improve the strengthening effect.

(4) Finally, based on the CAA and CA analytical models in the literature, considering the effect of CFRP sheets, the modified analytical models and construction measures for beams strengthened with CFRP sheets on the beam sides to mitigate progressive collapse of the RC frame are proposed. However, more tests should be carried out to further prove the accuracy of Equations (4) and (8).

Data Availability

The data that support the findings of this study are available from the corresponding author upon reasonable request.

Conflicts of Interest

The authors declare that they have no conflicts of interest.

Acknowledgments

This study was funded by the National Key Research Program of China (2016YFC0701400) and the Fundamental Research Funds for the Central Universities of China (NS2016018).

References

[1] X. Z. Lu, Y. Li, and L. P. Ye, *Theory and Design Method for Progressive Collapse Prevention of Concrete Structures*, China Architecture and Building Press, Beijing, China, 2011.

[2] B. R. Ellingwood and D. O. Dusenberry, "Building design for abnormal loads and progressive collapse," *Computer-aided Civil and Infrastructure Engineering*, vol. 20, no. 3, pp. 194–205, 2005.

[3] K. Qian, B. Li, and Y. Liu, "Integrity of precast concrete structures to resist progressive collapse," in *Proceedings of the Geotechnical and Structural Engineering Congress 2016*, Phoenix, AZ, USA, 2016.

[4] K. Qian and B. Li, "Performance of precast concrete substructures with dry connections to resist progressive collapse," *Journal of Performance of Constructed Facilities*, vol. 32, no. 2, article 04018005, 2018.

[5] S.-B. Kang and K. H. Tan, "Behaviour of precast concrete beam-column sub-assemblages subject to column removal," *Engineering Structures*, vol. 93, pp. 85–96, 2015.

[6] S.-B. Kang, K. H. Tan, and E.-H. Yang, "Progressive collapse resistance of precast beam-column sub-assemblages with engineered cementitious composites," *Engineering Structures*, vol. 98, pp. 186–200, 2015.

[7] R. B. Nimse, D. D. Joshi, and P. V. Patel, "Behavior of wet precast beam column connections under progressive collapse scenario: an experimental study," *International Journal of Advanced Structural Engineering*, vol. 6, no. 4, pp. 149–159, 2014.

[8] Y. Pan, X. H. Chen, Y. Y. Yao et al., "Progressive collapse analysis of unbonded post-tensioned precast RC frame structures using column removal method," *Engineering Mechanics*, vol. 34, no. 12, pp. 162–170, 2017.

[9] D.-C. Feng, G. Wu, and Y. Lu, "Numerical investigation on the progressive collapse behavior of precast reinforced concrete frame subassemblages," *Journal of Performance of Constructed Facilities*, vol. 32, no. 3, article 04018027, 2018.

[10] K. Qian and B. Li, "Strengthening and retrofitting of RC flat slabs to mitigate progressive collapse by externally bonded CFRP laminates," *Journal of Composites for Construction*, vol. 17, no. 4, pp. 554–565, 2013.

[11] K. Qian and B. Li, "Strengthening of multibay reinforced concrete flat slabs to mitigate progressive collapse," *Journal of Structural Engineering*, vol. 141, no. 6, article 04014154, 2015.

[12] I. S. Kim, J. O. Jirsa, and O. Bayrak, "Anchorage of carbon fiber-reinforced polymer on side faces of reinforced concrete beams to provide continuity," *ACI Structural Journal*, vol. 110, no. 6, pp. 1089–1098, 2013.

[13] J. Kim and H. Choi, "Monotonic loading tests of RC beam-column subassemblage strengthened to prevent progressive collapse," *International Journal of Concrete Structures and Materials*, vol. 9, no. 4, pp. 401–413, 2015.

[14] S. L. Orton, *Development of a CFRP System to Provide Continuity in Existing Reinforced Concrete Buildings Vulnerable to Progressive Collapse*, University of Texas at Austin, Austin, TX, USA, 2007.

[15] P. Feng, K. J. Shi, W. H. Qin et al., "Experimental study on progressive collapse behaviour of GFRP strengthened RC beam-column structures," in *Proceedings of National Construction Project FRP Application Academic Conference*, Harbin, China, 2013.

[16] H. Y. Zhang, *Experiment and Method on CFRP-Retrofitted RC Frames Damaged by Progressive Collapse*, Harbin Institute of Technology, Harbin, China, 2017.

[17] J. Yang, *Experimental Study by Using CFRP Laminates on Preventing Progressive Collapse of RC Frame*, Hunan University, Changsha, China, 2014.

[18] Y. A. Al-Salloum, M. A. Alrubaidi, H. M. Elsanadedy, and R. A. Almusallam, "Strengthening of precast RC beam-column connections for progressive collapse mitigation using bolted steel plates," *Engineering Structures*, vol. 161, pp. 146–160, 2018.

[19] Y. Pan, X. H. Chen, H. P. Wang et al., "Seismic fragility analysis of unbonded post-tensioned fabricated RC frame structures," *Journal of Harbin Institute of Technology*, vol. 50, no. 6, pp. 71–77, 2018.

[20] DBJT 08-116-2013, *Standard Drawings for Construction Joints of Assembled Monolithic Concrete Residential Buildings*, Shanghai Construction Engineering Design Research Institute, Shanghai, China, 2013.

[21] DoD 2010, *Design of Structures to Resist Progressive Collapse*, Department of Defense, Washington DC, USA, 2010.

[22] J. W. Zhang, L. J. Yue, Z. T. Lv et al., "Experimental study on the behavior of the strengthened RC beam side-bonded with CFRP sheets," *Journal of Southeast University*, vol. 32, no. 5, pp. 760–765, 2002.

[23] X. J. Chen, M. X. Dai, and Y. Xu, "Calculation and analysis on flexural capacity of RC beam strengthened with side-bonded FRP," *Journal of Yangtze River Scientific Research Institute*, vol. 28, no. 11, pp. 100–82, 2011.

[24] GB 50367-2013, *Code for Design of Strengthening Concrete Structure*, China Architecture and Building Press, Beijing, China, 2013.

[25] R. Park and W. L. Gamble, *Reinforced Concrete Slabs*, John Wiley & Sons, New York, NY, USA, 2000.

[26] Y. P. Su, Y. Tian, and X. S. Song, "Progressive collapse resistance of axially-restrained frame beams," *ACI Structural Journal*, vol. 106, no. 5, pp. 600–607, 2009.

[27] K. Qian, B. Li, and J.-X. Ma, "Load-carrying mechanism to resist progressive collapse of RC buildings," *Journal of Structural Engineering*, vol. 141, no. 2, article 04014107, 2015.

[28] J. Yu and K. H. Tan, "Analytical model for the capacity of compressive arch action of reinforced concrete sub-assemblages," *Magazine of Concrete Research*, vol. 66, no. 3, pp. 109–126, 2014.

[29] S.-B. Kang and K. H. Tan, "Analytical study on reinforced concrete frames subject to compressive arch action," *Engineering Structures*, vol. 141, pp. 373–385, 2017.

[30] X. Lu, K. Lin, and C. Li, "New analytical calculation models for compressive arch action in reinforced concrete structures," *Engineering Structures*, vol. 168, pp. 721–735, 2018.

[31] Y. Li, W. Botte, and R. Caspeele, "Reliability analysis of FRP strengthened RC beams considering compressive membrane action," *Construction and Building Materials*, vol. 169, pp. 473–488, 2018.

[32] W. J. Yi, Q. F. He, Y. Xiao et al., "Experimental study on progressive collapse-resistant behavior of reinforced concrete frame structures," *ACI Structural Journal*, vol. 105, no. 4, pp. 433–439, 2008.

[33] A. T. Pham and K. H. Tan, "A simplified model of catenary action in reinforced concrete frames under axially restrained conditions," *Magazine of Concrete Research*, vol. 69, no. 21, pp. 1115–1134, 2017.

[34] K. Alogla, L. Weekes, and L. Augusthus-Nelson, "Theoretical assessment of progressive collapse capacity of reinforced concrete structures," *Magazine of Concrete Research*, vol. 69, no. 3, pp. 145–162, 2017.

[35] J. F. Chen and J. G. Teng, "Anchorage strength models for FRP and steel plates bonded to concrete," *Journal of Structural Engineering*, vol. 127, no. 7, pp. 784–791, 2001.

[36] H. Zhang and S. T. Smith, "Fibre-reinforced polymer (FRP)-to-concrete joints anchored with FRP anchors: tests and experimental trends," *Canadian Journal of Civil Engineering*, vol. 40, no. 11, pp. 1103–1116, 2013.

[37] P. C. Li, *Experimental Study on the Performance of C/S HFRP Anchors*, Nanjing University of Aeronautics and Astronautics, Nanjing, China, 2017.